Micro-CT Imaging of Low-density Plant Stems

Bonita Van Heel
University of Minnesota Twin Cities Campus: University of Minnesota Twin Cities
Deborah Jo Heuschele (jo.heuschele@usda.gov)
USDA Agricultural Research Service https://orcid.org/0000-0002-8157-8458
Yiting He
Sun Yat-Sen University
Alex Fok
University of Minnesota Twin Cities Campus: University of Minnesota Twin Cities

Research Article

Keywords: Micro-CT, stems, contrast, low density, fixative

Posted Date: January 17th, 2022

DOI: https://doi.org/10.21203/rs.3.rs-1251568/v1

Abstract

Background

Micro-CT (X-ray computed tomographic) allows for 3D visualization of an entire structure, both internally and externally. The different materials are identified based on the differences in their ability to attenuate X-ray, with the differences being converted into a range of grey values. Low-density plant tissues with limited differences in grey values create a challenge in differentiating the cellular structures. In addition, internal movements due to autolysis, degradation, and shrinkage during dehydration of the tissues during scanning give rise to blurry images.

Results

In this study, oats and wheat were scanned using micro-CT to optimize the use of micro-CT in low-density plants. With the assistance of chemical fixing, phosphotunstate and a chemical drying agent, we were able to visualize microstructures of cereal stems. These preparation steps allow us to create 3D micrographs of low-density stem nodes suggesting key structural differences that are correlated with lodging resistance.

Conclusion

Micro-CT is a valuable tool to create 3D structural images of low-density material. Multiple steps to prepare the samples to stop autolysis, increase the contrast during scanning and eliminate internal movement are described in this paper. This process allowed for visualization of the stem nodal region suggesting morphology related to lodging resistance.

Background

Small grain cereals lose a high percentage of their yield through lodging (buckling of the stems near ground level) before harvesting due to the weak structure of the stem, especially under heavy rain and wind (1). Computational models are being used to simulate stem collapse under loads to better understand the relationship between the stem's structure and its strength (2). With this understanding, the stem's structure can then be modified through conventional breeding or genetic engineering to increase its resistance against lodging. However, to construct these models, three-dimensional (3D) structural images of the stem are required. 3D images can be carefully built from a limited number of individual 2D cross sections (3) of various types of microscopy. These resulting 3D models assume that the cross sections capture all the internal structure variation present and that those structures are continuous. If the assumption is incorrect, error is introduced into the computational models, resulting in large variations that do not mimic real-world results. Micro-CT however takes 2D image stacks from micro slices continuously through the plant stem to build a 3D model by measuring tissue density. This process

allows for the 3D visual reconstruction of structures such as anatomical vascular systems. Researchers can now study entire cellular structures to understand how cellular systems are constructed and morphometric parameters can be extracted. At this time, whole potted plants in-situ or intact plants cannot be used to achieve high resolution which is complicated by auto-digestion and liquid evaporation that causes blurry images due to internal movements within the plant (4). Therefore, adjusting sample size is needed to achieve high resolution. Micro-CT imagery has been used to visualize plant tissues of fruits (5), leaves (6) and pollen development (7) but not larger plant structures such as whole stems.

One of the largest challenges to using micro-CT imagery on larger plant and animal tissues is the low contrast between tissues and the environment (4). To some extent, image contrast is dependent on the micro-CT machine parameters, such as over exposure and how the x-ray attenuates the tissue (i.e. signal to noise ratio). However, due to the high radiolucency of organic matter or low density of plants, they do not readily lend themselves to micro-CT imaging. To enhance the contrast between solid and air in the images, absorbable contrast agents can be used to increase the radiopacity of the organic matter (8). In order for some contrast agents to penetrate and bind to the tissues, proper prior fixation needs to occur.

There are three main ways fixatives can be divided, coagulant vs non-coagulant, additive vs non-additive or acidic vs basic vs aldehyde (9). The key to all these fixatives is how they interact with the plant tissue. Research goals as well as the plant biology dictate which fixative type is most applicable for the study. In the case of micro-CT imagery, only cell wall boundaries are of interest. Consequently, fixatives that retain cytosolic microstructures are not needed. Conversely, fixatives that increase shrinkage due to water loss might alter certain plant cell wall structures and therefore be inadvisable. These chemicals remove and replace free water in cells and tissues and cause a change in the tertiary structure of proteins by destabilizing hydrophobic bonding (10). Fixatives that are coagulants or have additive properties (stay embedded into the cell wall) should be tested with any contrasts to determine if there are any contrast agent clumping or interfering with clear structural cell wall differentiation. With the correct combination of fixative and contrast, a clear distinction between cell walls can be determined. Information resulting from these techniques can be applied to computational models such as to theorize how and why structures bend and some break (11).

In this paper, we developed a method to evaluate low-density tissue of herbaceous stems to determine structural differences that might lead to lodging resilience. Outlined is the process to determine the correct combination of fixing agent and contrast to visualize two distinct segments (Fig. 1) of the low-density wheat and oat stems along with the use of a chemical drying agent to prevent autodigestion and dehydration during scanning.

Results/discussion

The goal of this study was to determine a more direct time saving method to visualize stems of cereals for cellular wall structure comparisons using 3D micro-CT imaging.

Optimization

Micro-CT imaging of plants can be challenging due to the low level of x-ray absorption of the tissues (12). Our initial micro-CT (XT H 225, Nikon Metrology Inc., Brighton, MI, USA) scanning parameters were 75 kV tube voltage, 75 µA tube current, 708 ms exposure time, 720 projections and 4 frames per projection. The total scanning time was approximately 35 min for each specimen. The resulting images were grey, blurry, and undefined with no cell boundary details and limited contrast (Fig. 2: B & C). Only one peak was formed (Fig. 2A). Lowering the x-ray energy and exposure time for each sample improved the resolution in the low-density herbaceous plant tissue. Adjusting scanning parameters to optimal settings of 100 kV, 40 uA and exposure time of 354 with a magnification of 33.05 gave us a voxel size of 4.05 microns and resulted in a second peak in the grayscale (Fig. 2D). This second peak indicated a successful separation of the sample from the background (Fig. 2D) which would allow the tissues to be isolated using a suitable grey-value threshold (Fig. 2: A & D). The number of projections used was 360, with 16 frames per projection. These settings provided a good signal-to-noise ratio. No filter was used for the X-ray beam because it did not improve the quality of the scans.

To further widen the grey scale and to improve visibility of details, we introduced a commonly used contrast agent (Hexibrix 12.5% (v/v) Guerbet LLC, Bloomington, IN, USA) through a fresh stem using capillary action. Stem segments (3-5 cm) were partially embedded into the foam and filled with 400 ml of Hexibrix. The foam helped stabilize the stem for scanning. However, the contrast agent did not penetrate the stem section; contrast only coated and clumped on the outside surface. In addition, the physical stem length needed to be reduced for higher resolution. Optimized machine parameters included bringing the sample closer to the target resulting in a magnification of 33.05 and a voxel size of 4.05 µm. A straight stem segment with a diameter of 0.5-1 cm and length between 3-5 cm increased the likelihood of the 3D reconstruction software to identify the center of rotation.

After machine optimization, the samples remained blurry, possibly due to auto digestion and interior movement through liquid evaporation (13). Cellular degradation on a micro level during the duration of the scan is reasonable (i.e. evaporation), therefore, it was necessary to fix the tissues to preserve the morphological and molecular features of the tissue. We tested fixatives to assist in dehydrating the stems prior to imaging. In addition, the ability for a contrast agent to penetrate the cellular structures is dependent on proper fixation of the plant tissues (10, 14). Fixative selection is important, as there can be an interaction due to crosslinking between the fixatives and contrast agents (15). This interaction can cause the clumping of contrast in the tissues. The optimal combination of fixing and contrast agent to use are ones that have similar pH values (16). Not one individual fixative was recommended or preferred over another in the literature; therefore, we compared the images of samples prepared using four acidic fixatives. After the stems were cut to the appropriate size, they were immediately placed into 1.5-mL micro-centrifuge tubes, filled with one of the following four fixing agents: 70% ethanol (ETOH), formaldehyde alcohol acetic acid (FAA), Farmer, and Carnoy's (Supplementary Table 1). All samples used fresh fixatives and no vacuum was applied during fixation. The samples were then stored at 4°C in fixative solution overnight and scanned the following day.

The addition of contrast improved the x-ray attenuation. Capillary action in a desiccator did absorb some of the contrast but it was insufficient to penetrate all the stem tissue. Different tissue reactions materialized according to the combination of fixative and contrast agent and the density of the tissues; one-day soak was sufficient for absorption of contrast after fixation to increase the x-ray attenuation into the internode whereas a two-day soak in contrast was needed for the thicker node material (Fig. 3 & 4). This difference is due to changes in the cross-linking of the fixative-contrast combinations within the organic tissue. These compounds bind to a variety of chemical groups in the tissues, often affecting the charge at the site of attachment (15). The internodal tissues fixed with FAA and Carnoys with contrast (Osmium Tetroxide or Phosphotungstate) were comparable (Fig. 3 & 4). When two combinations give comparable results, it is important to use the least toxic combination. The combination of FAA and phosphotunstate resulted in better images for the node sections while Carnoy's and phosphotunstate worked better for the internode sections. FAA was chosen for its ability to absorb into the high-density cells (nodes) allowing the contrast to penetrate and distribute evenly. Even though FAA and Carnoy's were comparable for the internodes, Carnoy's seemed to have better distribution of the contrast within the internodal tissues. There was no difference in x-ray attenuation between the two contrast agents; therefore, we chose to use phosphotunstate over osmium tetroxide because it was less toxic.

To further ensure the removal of all water out of the cells, the tissue was chemically dried with hexamethyldisilane (HMDS) (Fig. 3). Plant stems required a longer dry time then previously recorded (16). This phenomena may be because the structure of plant cell walls impedes water loss. Therefore, allowing the chemical drying agent to fully evaporate from the plant under the hood was required. The introduction of contrasting agents and chemical drying increased the signal to noise ratio of the grey values to above 100 with the peak just under 300 in both the node and internode (Fig. 5E & 6E). This process allowed the plant tissue to stop the auto digestion, absorb the contrast agent uniformly and dry the tissue. Internal structures such as the vascular tissue could now be differentiated.

Validation

The optimized micro-CT images were compared with environmental SEM (TM-3000, Hitachi, High-Technologies Corporation, Tokyo, Japan) images of paired stem sections. Similar levels of detail can be seen (Fig. 5 & 6) between the micro-CT and SEM 2D images. Both methods could differentiate between cell primordia within the parenchyma tissues. The successful separation of the cellular boundaries within the micro-CT images permits the study of the spatial organization of the tissues and allows for detailed 3D micro-CT images to be created. The resulting 3D images were used to develop a sophisticated 3D numerical model to predict structural behaviors (2).

Analysis of plant tissue

We believe this is the first time cereal nodal structures have been 3D imaged in detail. Niklas (17) discussed the physics for nodes in detail, but only described them as septa or diaphragm like. The introduction of transverse septa or nodes to the hollow tube increases the strength and flexibility of the tube-shaped stem (Fig. 1). These struts reduce the tube length, thereby, reducing regionally increasing

stiffness of the tube. Nodes, solid amorphous tissue connecting long stem segments, can increase stiffness as much as 16 – 20%, even though they only contribute about 2% of the total stem weight (Niklas 1989). The internode, long segments of the stem, has the characteristic distribution of the strengthened tissues like vascular bundles equally distributed as far from the stem axis as possible with a hollow pneumatic center (18).

The micro-CT images allowed for clear visualization of cellular boundaries. The mechanical, parenchyma and lumen areas have distinct densities that are visualized by the micro-CT (Fig. 7). We did not find a statistical difference between the overall oat and wheat stem diameter ($p=0.18$). However, the thickness of the mechanical layer changed in size between species. This result has been seen between various wheat genotypes (19). Wheat clearly had larger vascular bundles composed of sclerenchyma in the mechanical layer, which could contribute to increased internodal strength compared to oat (20). Grasses, like cereals, use cylindrical geometry to maximize their strength and flexibility with the least amount of cellular tissue. A cylinder and to a greater extent, a hollow tube, is the most efficient geometric form to resist bending, elastic buckling, and torsion (21). Therefore, it is not surprising that plants use variations of this geometry in their growth.

In both cereals, two distinct rings separate from each other during scan preparation (Fig. 7D & H). The outer ring is not continuous, unlike the inner ring; an area can be clearly seen where the outer ring begins wrapping around the inner ring. This phenomenon is not noted in studies that used fresh material (22–25). The ring alignment overlap can be seen in the 2D cross sections of the micro-CT scans (Fig. 7D & H). This overlap could be an artifact from the direction in which the cells form the apical meristem align during development. A spiral pattern can be seen clearly during growth at the seedling stages, where oat at leaf arrangement is clockwise while wheat's is counterclockwise.

Lateral and 3D images show various specialize structures with-in the nodal tissue that vary between species. First, oat nodes were found to be dense throughout the entirety of the nodal structure (Fig. 7A-C) while wheat contained large air pockets surrounding a center pith (Fig. 7E). These air pockets can also be seen on the lateral view (Fig. 7F & G). Secondly, the inner and outer thickness of nodal diaphragm or septa differed between oat and wheat ($p= 0.031$). The thinnest section of the nodal diaphragms is significantly greater in oat (1.94 ± 0.1 mm) (Fig. 7B & C) than wheat (1.58 ± 0.12mm) (Fig. 6F & G). The outer thickness of the node is also greater in the oat (2.94 ± 0.2 mm) than wheat (2.35 ± 0.3 mm). The nodes act as spring-like joints (26) where the spring constants of the nodes are directly related to the natural frequencies of vibration of the stems when set in motion (21, 26, 27). The differences in the thickness of the nodal diaphragms results in different spring constants. Wheat contains a lighter "spring" that is flexible, while the oat "spring" is thick and stiff. Wheat also contains equally spaced air spaces resembling flat discs that compress without damaging cellular tissue to add more flexing capabilities within the node (Fig. 7E-G). These multiple pneumatic air spaces and mechanical structures add additional strength (18).

Within a flexed grass stem, total strain energy is divided between the nodal diaphragms and the internodal walls where both structural elements operate as a single mechanical system (28). The internodal walls provide rigidity and strength, while the nodes contribute flexibility. The cellular makeup and distribution pattern of those cells is different for each structure.

Conclusions

This method has been developed to visualize in 3D, low-density organic matter using micro-CT. Effective fixative and contrast combinations are dependent on tissue cell density and chemical crosslinking with reactive cell components. However, when various fixative and contrast mixes result in equal x-ray attenuation, a less toxic choice should be made. The complete drying of the cellular tissues is required to prevent evaporation during the scan that can cause internal movement and results in undefined cellular details. We found for the determination of cell wall boundaries, this method is as accurate as SEM and produces 3D images over the length of stems. For the first time the detailed 3D rendering of nodal tissue, with the aid of micro-CT imaging, allowed researchers to quantitatively study the interaction between the node and internode tissue.

Methods

Plant Material

Greenhouse grown oat (*Avena sativia*) “Gopher” plants were used for optimizing the micro-CT scanning parameters for stem segments, while field grown oat and wheat (*Triticum aestivum*) “Linkert" used for structural comparisons. All plants were scanned one week after flowering. Well grown main stems were selected from each plant for all experiments. Optimization of parameters were replicated four times. Four plants per species were used for comparison of plant structural morphology. All stems were carefully cut into 3-5cm lengths using a new razor blade to prevent crushing of the stem edges sub-setting segments into nodes and internodes for imaging (Fig. 1).

Optimization of Sample Preparation

Straight stem sections, both nodes and internodes, of diameter 0.5 - 1 cm were selected from the main stem of a well grown plant. The large sections were carefully cut into sections of 2-3 cm long and then immediately placed into 15-mL micro-centrifuge tubes. Node and internode sections were submerged in four different fixatives at a concentration of 1:20 (wt./v tissue to fixative) and stored overnight at 4°C (Sup Table 1) Then samples were transferred to a new 1.5-mL centrifuge tube filled with 1 ml of phosphotungstate contrast agent and stored in the refrigerator at 4°C for an addition 1-2 days depending on the experiment. After removing samples from the contrast agent, the stem sections were rinsed with 25mM sodium phosphate solution (Na2HPO4 (99+%, Acros Organics, New Jersey, USA) three times. The stem segments were then dried using the optimized drying method.

Micro-CT Parametrization

Greenhouse grown oat segments were secured onto a Teflon stage holder using Cyanoacrylate (Scotch Super Glue, 3M Company, St. Paul, MN) and Zapit Accelerator (Dental Ventures of America, Inc., Corona, CA) to minimize vibration during scanning. Micro-CT machine (XT H 225, Nikon Metrology Inc., Brighton, MI, USA) with the following settings was used to collect images: exposure time (354 ms), tube acceleration voltage (100 kV), and tube current (40 µA). The samples were brought as close to the target as possible to maximize image resolution. Straight stem sections were used to allow the center of rotation to be identified readily in 3D reconstruction. The images were reconstructed using 3D CT Pro 3.3 (Nikon Metrology, Inc., Brighton, MI, USA) and visualized using VG Studio MAX 3.2 (Volume Graphics GmbH, Heidelberg, Germany). The same magnification was used for all samples

Scanning Electron Microscopy (SEM) Environmental

A table-top environmental scanning electron microscope (TM-3000, Hitachi, High-Technologies Corporation, Tokyo, Japan) was used to obtain scans for complementary fresh stem segments to determine how detailed the micro-CT images could be. The SEM images were used to compare CT images for a more detailed understanding of tissue microstructures. Equivalent stem segments to those imaged by micro-CT of nodes and internodes were selected to obtain SEM images of their transverse sections. The tissues were secured onto an SEM holder using SEM mounting carbon conductive tabs (Ted Pella Inc. Redding, CA USA). The holder containing the sample was placed on a stage in the SEM machine and scanning was performed under compo mode, the mode that could differentiate materials with different densities, with an accelerating voltage of 15 kV.

Trait Measurements and Statistics

Structural measurements of four oat and four wheat samples were extracted from their micro-CT images using VG Studio MAX 3.2 (Volume Graphics GmbH, Heidelberg, Germany). Internode cross sections were measured for stem wall thickness, and inner and outer shell thicknesses (Fig S1). The ratio between the inner and outer shell thicknesses were calculated. Node longitudinal sections were measured for total internal node height and height of the nodal diaphragm (Fig S1). After scanning, a subset of stems were sliced and internal measurements were verified using a light microscope (DP71, Olympus America Inc, PA).

ANOVA and Tukey HSD were conducted between oat and wheat for all traits using JMP Pro 14.2.0 software (SAS Institute Inc., Cary, NC, USA, 1989–2019).

Declarations

Ethics approval and consent to participate

Not applicable

Consent for publication

Not applicable

Availability of data and materials

The datasets used and/or analyzed during the current study are available from the corresponding author on reasonable request.

Competing interests

The authors declare that they have no competing interests. The authors declare that the research was conducted in the absence of any commercial or financial relationships that could be construed as a potential conflict of interest. Mention of trade names or commercial products in this publication is solely for the purpose of providing specific information and does not imply recommendation or endorsement by the U.S. Department of Agriculture. The USDA is an equal opportunity provider.

Funding

This research was supported in part by grants from Minnesota Department of Agriculture Grant No. 122130, UMN Rapid Agricultural Response Fund Grant No. AES00RR234

Authors contributions

JH conceived of the study and helped to draft the manuscript. BV and YH participated in its design and carried out the design of the study. JH performed the statistical analysis. JH, AF and BV participated in the sequence alignment and drafted the manuscript. All authors read and approved the final manuscript.

Acknowledgements

We thank D. von Ruckert and T. Gangwar for experimental and plant growth assistance and Mike Weston for making sample holders.

References

1. Berry P, Sterling M, Spink J, Baker C, Sylvester-Bradley R, Mooney S, et al. Understanding and reducing lodging in cereals. Advances in agronomy. 2004;84(04):215-69.
2. Gangwar T, Heuschele DJ, Annor G, Fok A, Smith KP, Schillinger D. Multiscale characterization and micromechanical modeling of crop stem materials. Biomechanics and Modeling in Mechanobiology. 2021;20(1):69-91.
3. Jung HG, Engels FM. Alfalfa Stem Tissues: Cell Wall Deposition, Composition, and Degradability. Crop Science. 2002;42(2):524-34.
4. Karunakaran C, Lahlali R, Zhu N, Webb AM, Schmidt M, Fransishyn K, et al. Factors influencing real time internal structural visualization and dynamic process monitoring in plants using synchrotron-based phase contrast X-ray imaging. Scientific Reports. 2015;5(1):1-13.

5. Herremans E, Verboven P, Verlinden BE, Cantre D, Abera M, Wevers M, et al. Automatic analysis of the 3-D microstructure of fruit parenchyma tissue using X-ray micro-CT explains differences in aeration. BMC plant biology. 2015;15(1):1-14.
6. Schneider JV, Rabenstein R, Wesenberg J, Wesche K, Zizka G, Habersetzer J. Improved non-destructive 2D and 3D X-ray imaging of leaf venation. Plant methods. 2018;14(1):1-15.
7. Tracy SR, Gómez JF, Sturrock CJ, Wilson ZA, Ferguson AC. Non-destructive determination of floral staging in cereals using X-ray micro computed tomography (μCT). Plant Methods. 2017;13(1):1-12.
8. Wang Z, Verboven P, Nicolai B. Contrast-enhanced 3D micro-CT of plant tissues using different impregnation techniques. Plant methods. 2017;13(1):1-16.
9. Ruzin SE. Plant microtechnique and microscopy: Oxford University Press New York; 1999.
10. Rolls G. Fixation and fixatives (2)– factors influencing chemical fixation, formaldehyde and glutaraldehyde. Leica Biosystem Wetzlar, Germany. 2012.
11. Gangwar T, Schillinger D. Microimaging-informed continuum micromechanics accurately predicts macroscopic stiffness and strength properties of hierarchical plant culm materials. Mechanics of Materials. 2019;130:39-57.
12. Mathers AW, Hepworth C, Baillie AL, Sloan J, Jones H, Lundgren M, et al. Investigating the microstructure of plant leaves in 3D with lab-based X-ray computed tomography. Plant methods. 2018;14(1):1-12.
13. Korte N, Porembski S. Anatomical analysis of turgescent and semi-dry resurrection plants: The effect of sample preparation on the sample, resolution, and image quality of X-ray micro-computed tomography (μCT). Microscopy research and technique. 2011;74(4):364-9.
14. Staedler YM, Masson D, Schönenberger J. Plant Tissues in 3D via X-Ray Tomography: Simple Contrasting Methods Allow High Resolution Imaging. PLoS ONE. 2013;8(9):e75295.
15. Rolls G. Process of Fixation and the Nature of Fixatives. Fixation and Fixatives Retrieved. 2012;20(06):2014.
16. Shively S, Miller WR. The use of HMDS (hexamethyldisilazane) to replace critical point drying (CPD) in the preparation of tardigrades for SEM (scanning electron microscope) imaging. Transactions of the Kansas Academy of Science. 2009;112(4):198-200.
17. Niklas KJ. Nodal septa and the rigidity of aerial shoots of Equisetum hyemale. American Journal of Botany. 1989;76(4):521-31.
18. Schulgasser K, Witztum A. On the strength of herbaceous vascular plant stems. Annals of Botany. 1997;80(1):35-44.
19. Packa D, Wiwart M, Suchowilska E, Bienkowska T. Morpho-anatomical traits of two lowest internodes related to lodging resistance in selected genotypes of Triticum. International agrophysics. 2015;29(4).
20. Gangwar TS, Alexander; Baranova, Svetlana; Guala, Michele; Smith, Kevin P.; Heuschele, D. Jo. Multiscale modeling predicts plant stem bending behavior in response to wind to inform lodging

resistance. Journal of the Royal Society. 2022.
21. Niklas KJ. Plant biomechanics: an engineering approach to plant form and function: University of Chicago press; 1992.
22. Kokubo A, Kuraishi S, Sakurai N. Culm strength of barley: correlation among maximum bending stress, cell wall dimensions, and cellulose content. Plant physiology. 1989;91(3):876-82.
23. Hamilton D. Culm, crown and root development in oats as related to lodging. Scientific Agriculture. 1951;31(7):286-315.
24. BROCK PBKAG. Structural Development of the Oat Plant. 1992.
25. O'keeffe L, Callenbach J, Lebsock K. Effect of culm solidness on the survival of the wheat stem sawfly. Journal of Economic Entomology. 1960;53(2):244-6.
26. Niklas KJ. Responses of hollow, septate stems to vibrations: biomechanical evidence that nodes can act mechanically as spring-like joints. Annals of Botany. 1997;80(4):437-48.
27. Niklas KJ, Moon FC. Flexural stiffness and modulus of elasticity of flower stalks from Allium sativum as measured by multiple resonance frequency spectra. American Journal of Botany. 1988;75(10):1517-25.
28. NIKLAS KJ. Modes of mechanical failure of hollow, septate stems. Annals of botany. 1998;81(1):11-21.

Tables

Table 1. Fixative, contrast, and rinse formulations

Fixatives	Contrast Agents	Rinse
FAA: 50 ml…100% Ethanol 10 ml … 37% Formaldehyde 5 ml …Glacial acetic acid 35 ml…Distilled H20 (This equals 100 ml solution)	**Osmium Tetroxide 2.5% w/v:** 0.25 g… Osmium Tetroxide 10 ml… Distilled H20	**Rinse:** Na_2HPO4 (25mM) 40ml = 0.142 g (Na_2HPO4 powder) + 40 ml of H2O
Carnoy's: 1-part Glacial Acetic Acid 3-parts Chloroform 6-parts 95% or absolute (100%) Ethanol	**Phosphotungstate 5% w/v:** 0.5 g… Phosphotungstate 10 ml…Ethanol (95%)	
Farmers solution 1-part Glacial Acetic Acid 3-parts 95% Ethanol		
70% Ethanol		

Figures

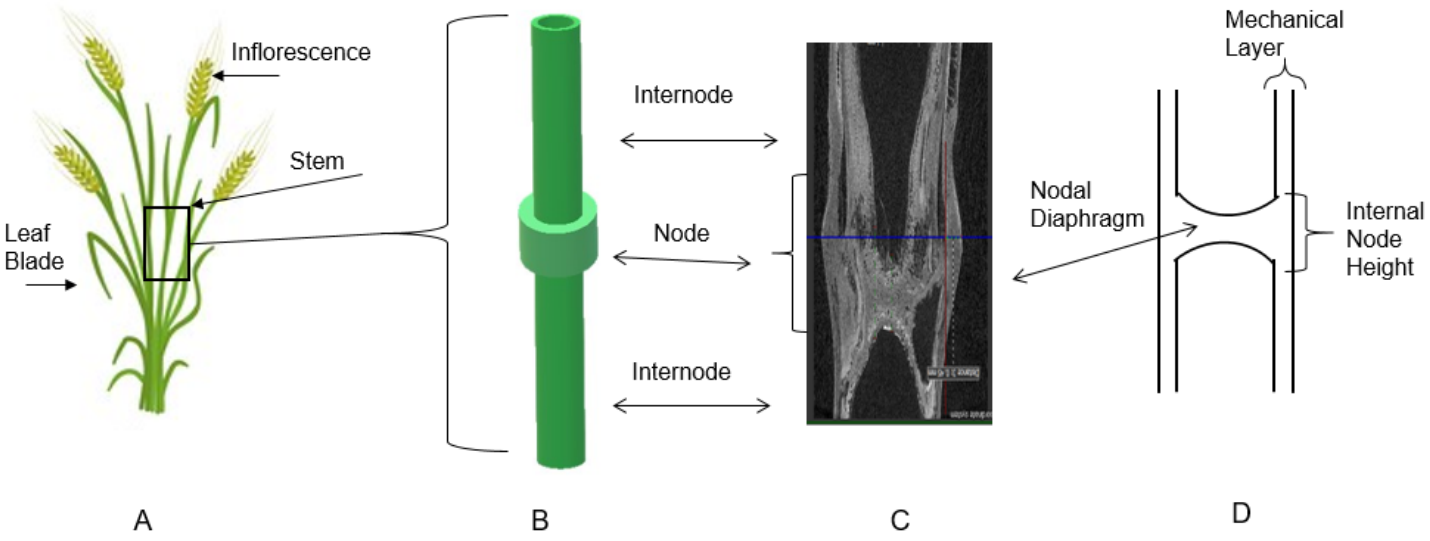

Figure 1

Typical anatomy of a small grain plant. A) Whole plant B) Stem structures C) micro-CT image of internode and nodal region D) internal structure of the nodal region.

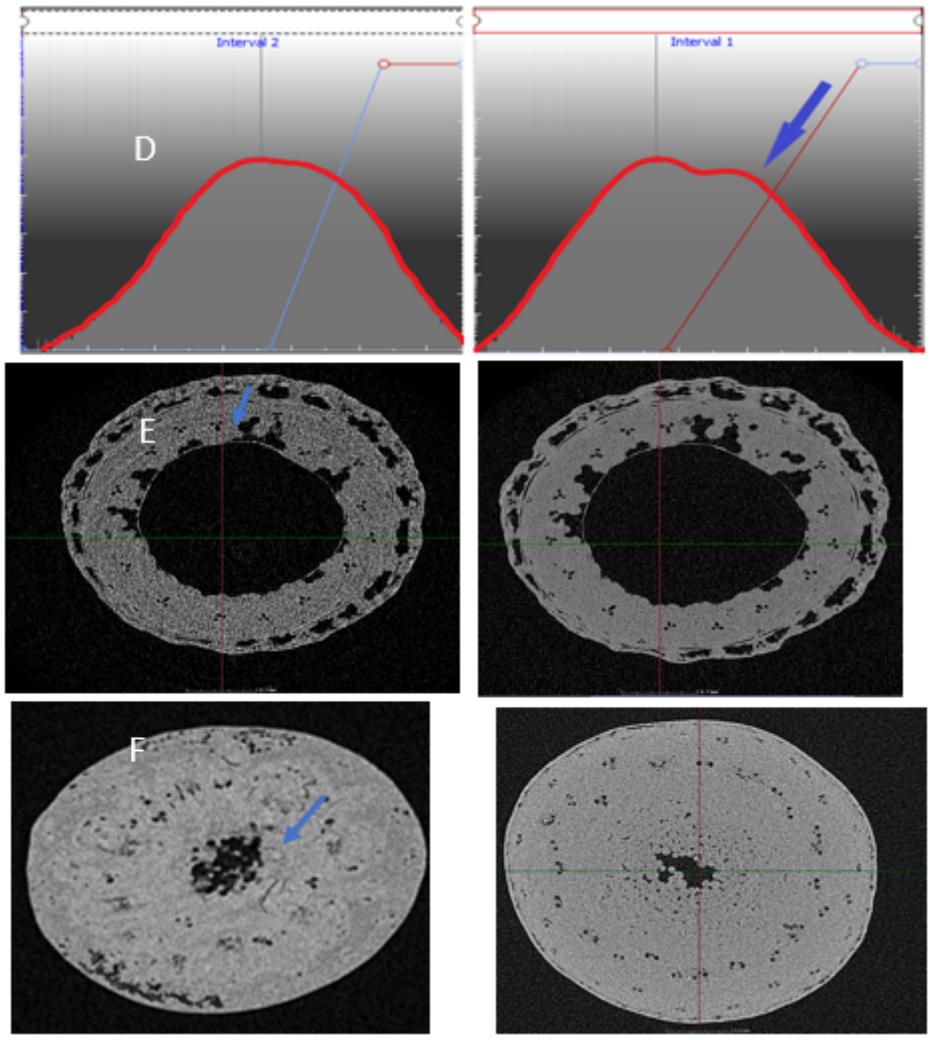

Figure 2

Micro-CT images before and after machine adjustments to improve image quality.

A) Initial setting resulted in one grey value peak. B & C) Internode and node before parameter adjustments. Yellow arrows show lack of cellular detail, and no defined boundaries. Images are blurry. D) The blue arrow indicates a second peak in the histogram. After lowering the current from 48 to 40 uA and selecting a higher frame rate per projection the separation of material is now possible. Images E & F) internode and node after adjusting machine parameters. Blue arrow show cellular boundaries and cell clusters.

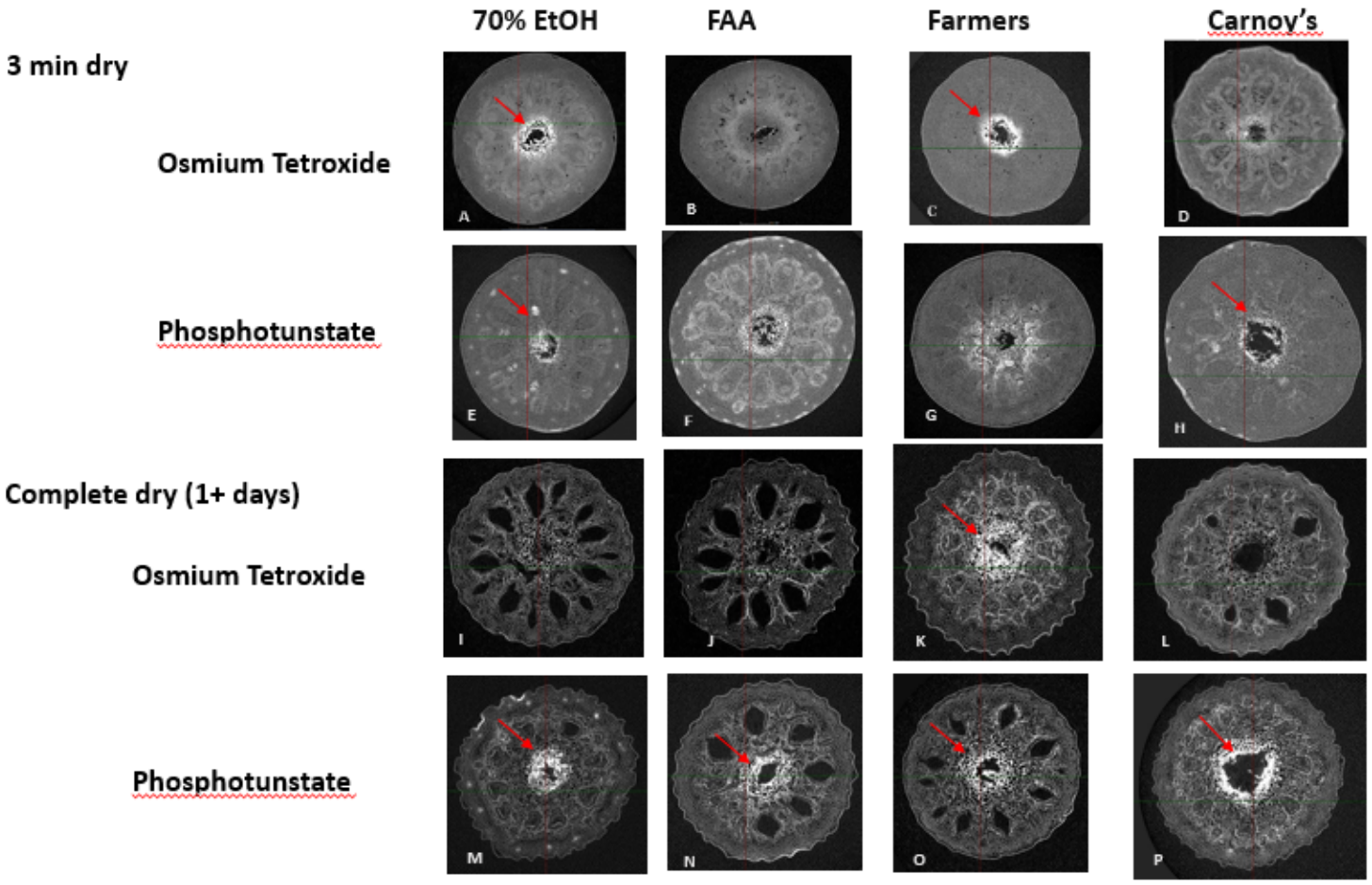

Figure 3

Fixed nodes with different contrast immersion times (method I, one hr. or method II, two days) with different HMDS drying times.

A visual comparison between the different combinations were made taking into consideration absorption, distribution and clarity. A-H were immersed in contrast for 1 hr. (Osmium Tetroxide or Phosphotungstate). Samples A – H all have insufficient absorption and distribution of contrast agent. A, C, E, G, H combinations of fixatives and contrast agents have bright areas in the center clinging to the lignin in the center of the tissue (See red arrows).

K, M, N, O & P have a concentrated amounts of contrast agent in the center area of the sample. J (FAA with Phosphatungstate) was chosen as the preferred combination of fixative and contrast agent.

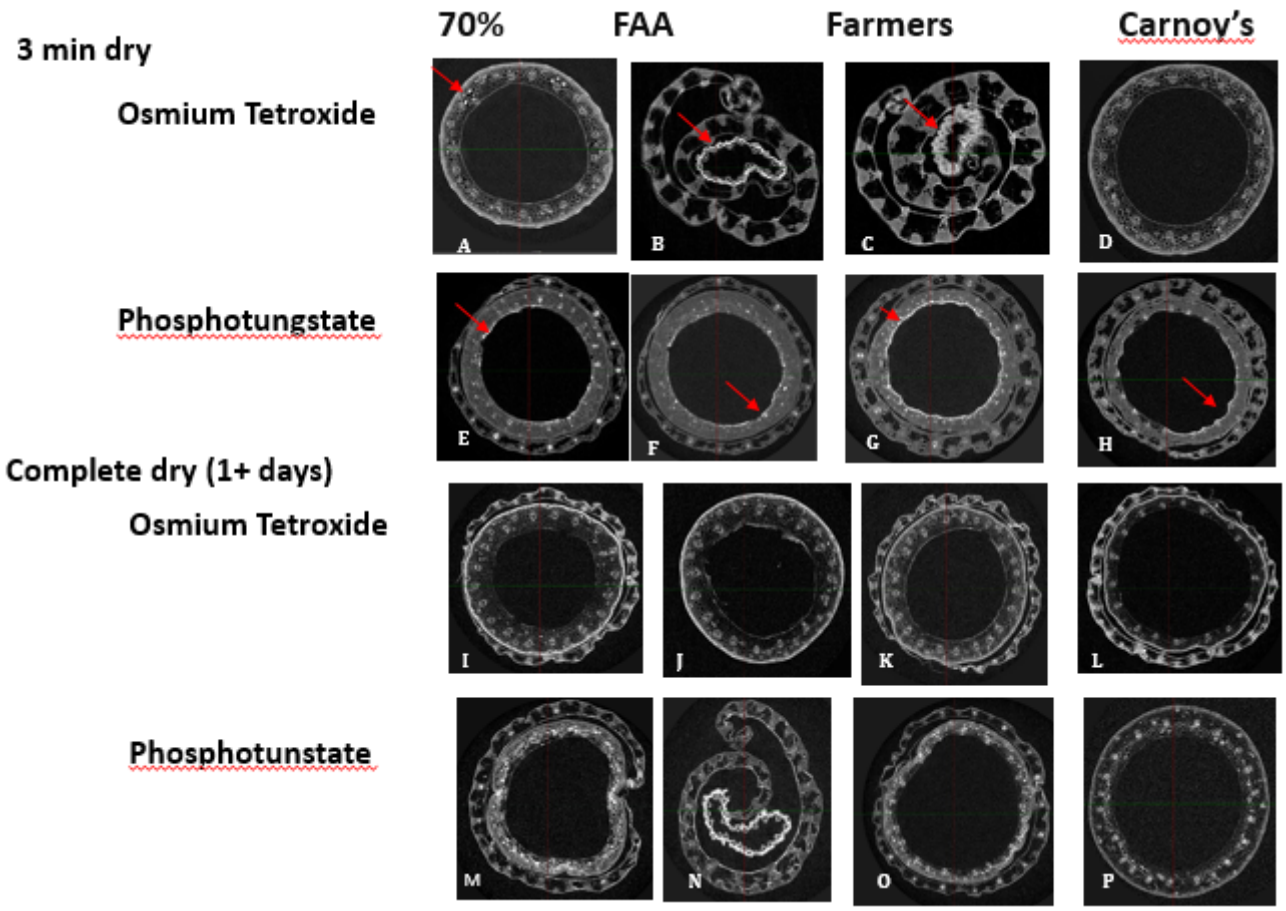

Figure 4

Visual comparisons of internodes with different contrast immersion times and different HMDS dry times (fast dry method I and slow dry method II).

A-H) were immersed in contrast for 1 hour (Osmium Tetroxide or Phosphotungstate) and dried with HMDS for 3 minutes. Samples A-C & E-H combinations of fixative and contrast agent have bright areas where the contrast agent clings to the tissue in clumps indicated by the red arrows. D & H) have the least amount of clumping. I-P) *Contrast immersion time and the HMDS dry time was increased to 1 day and completely dried with total evaporation of HMDS. P) (Carnoy's with Phosphatungstate) was chosen as the preferred combination of fixative and contrast agent over J due to the toxicity of osmium tetroxide.*

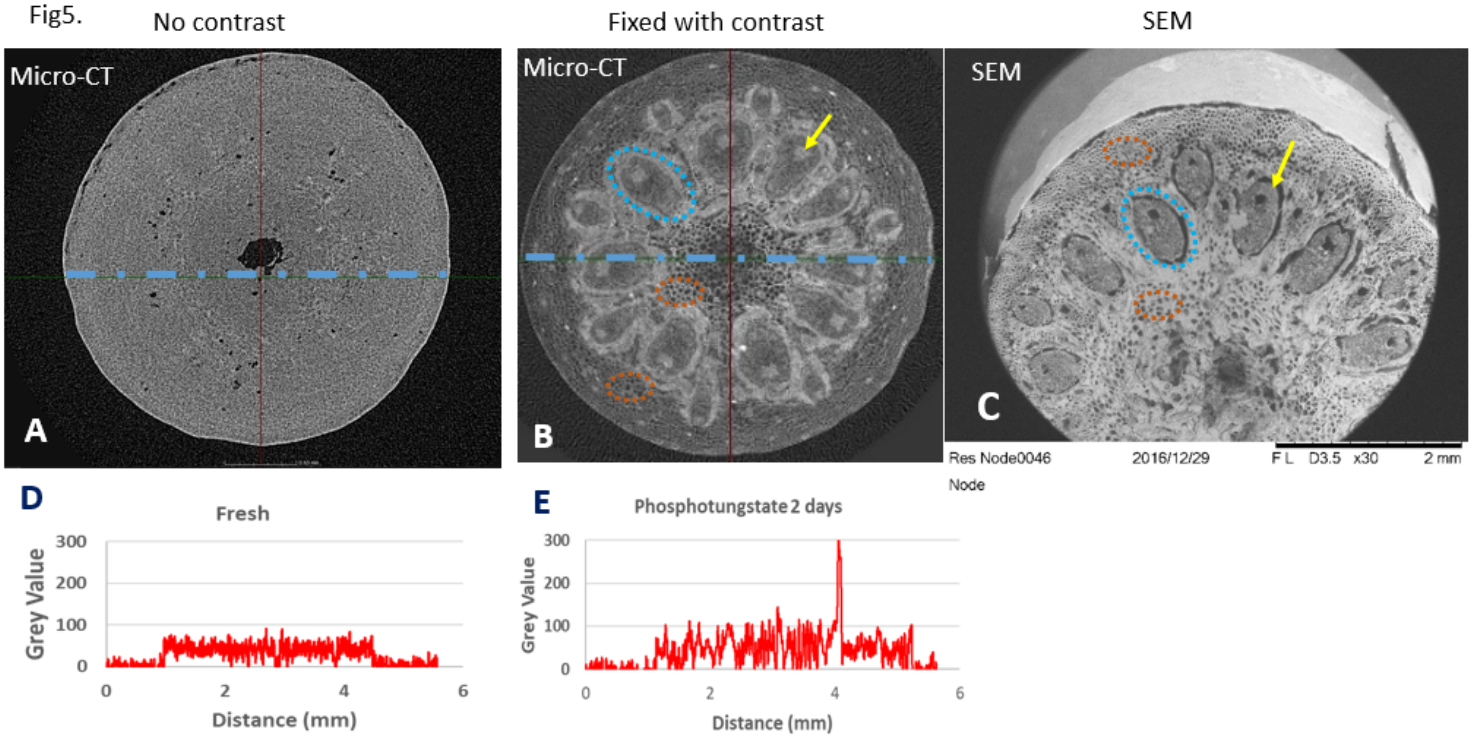

Figure 5

Micro-CT node comparisons with high resolution SEM image and exported grey values.

A) is a node with no contrast and no defined cellular boundaries. B) Micro-CT image of node defined cellular boundaries and identifiable structures as shown with the blue and orange dotted oval circles. The blue line in images (A and B) is the distance of the cross section of the exported grey values E and D. C) is a high-resolution SEM image of a node with comparable identifiable structures shown with blue and orange dotted circles. The yellow arrows are vascular bundles.

D) The node without using a contrast agent has grey values under 100.

E) The node immersed in Phosphotungstate for 2 days and dried in HMDS shows an increase of grey value distributed throughout the node from below 100 to a peak of 300.

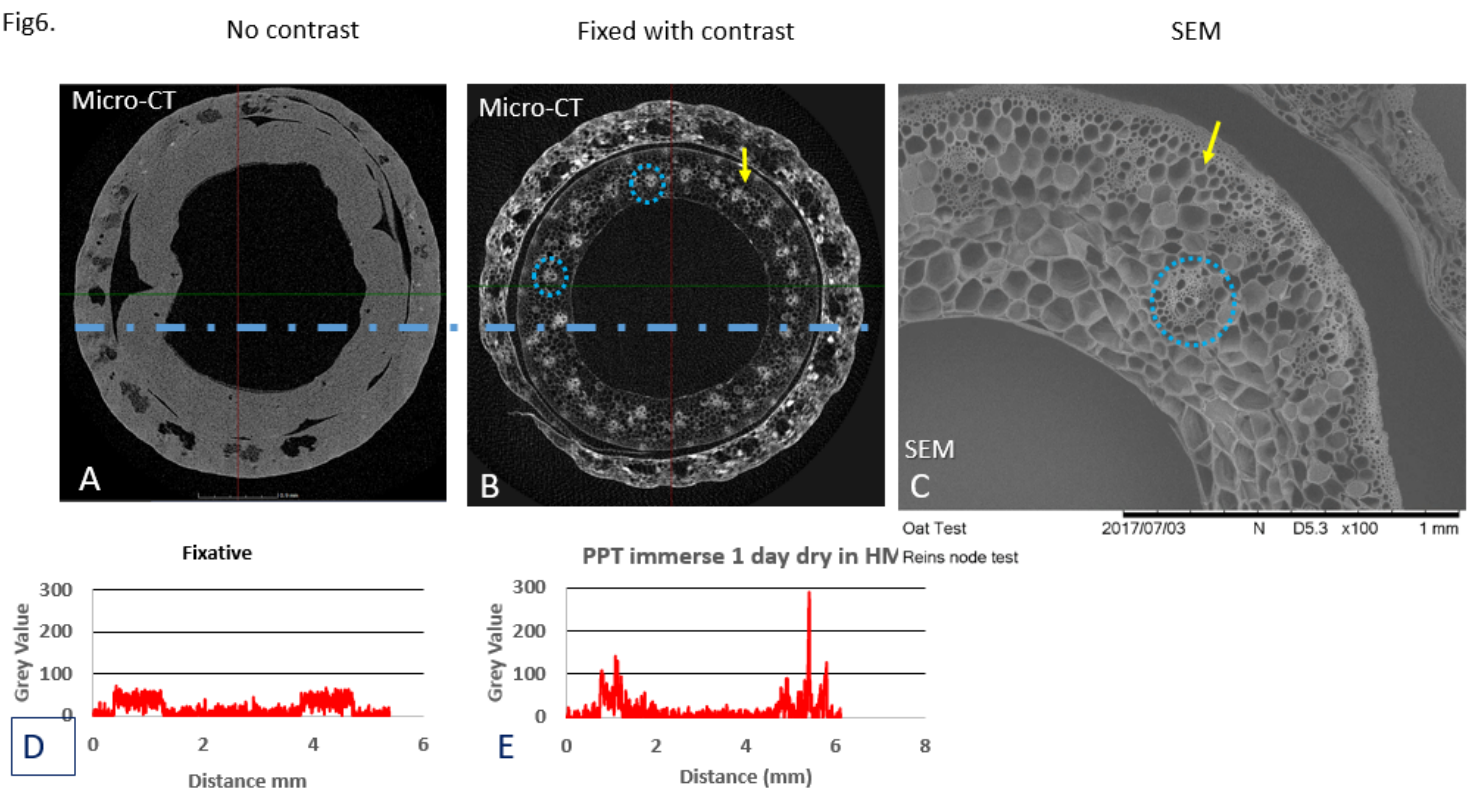

Figure 6

Micro-CT internode comparisons with high resolution SEM image and exported grey values.

A) Node with no contrast and no defined cellular boundaries. B) Micro-CT image of node showing defined cellular boundaries and identifiable structures as indicated with the blue and orange dotted oval circles. The blue line in images A & B is the distance of the cross section of the exported grey values E and D. C) High-resolution SEM image of a node with comparable identifiable structures shown with blue dotted circles. The yellow arrows are ground tissue.

D) The node without using a contrast agent the grey values are under 100.

E) The node immersed in Phosphotungstate for 2 days and dried in HMDS shows an increase of grey value distributed throughout the node from below 100 to a peak of 300.

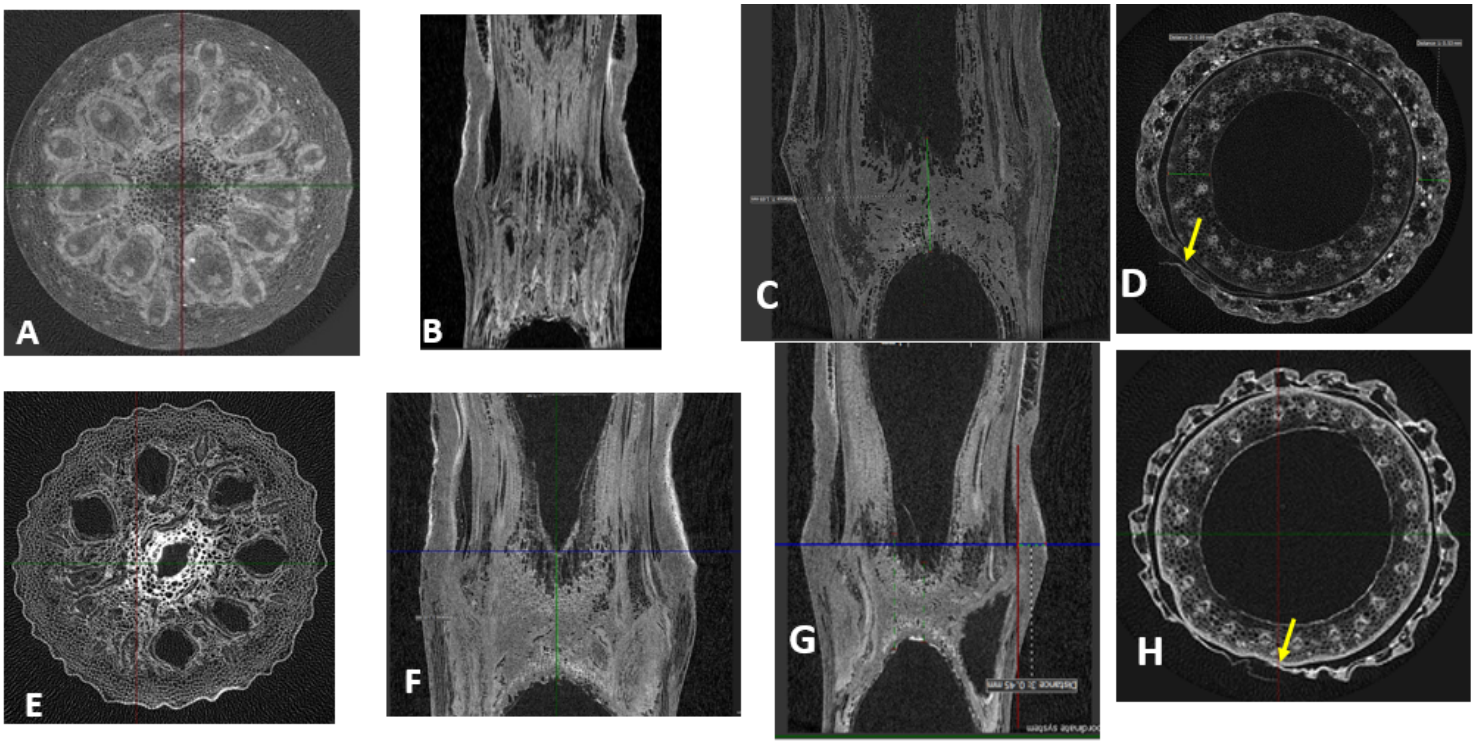

Figure 7

Comparison of node and internode structure of oat and wheat.

A- D) oat E-H) wheat, B & F) longitudinal cross - section at edge node, C & G) longitudinal cross-section at mid point of node. D & H) internode cross-section. Yellow arrows indicate overlapping outer ring.

Supplementary Files

This is a list of supplementary files associated with this preprint. Click to download.

- SupplementaryFigure1.png